CHIN. PHYS. LETT. Vol. 36, No. 5 (2019) 050301

Implementation of Full Spin-State Interferometer *

Peng-Ju Tang(唐鹏举)[1], Peng Peng(彭鹏)[1], Xiang-Yu Dong(董翔宇)[1], Xu-Zong Chen(陈徐宗)[1], Xiao-Ji Zhou(周小计)[1,2]**

[1]*State Key Laboratory of Advanced Optical Communication System and Network, School of Electronics Engineering and Computer Science, Peking University, Beijing 100871*

[2]*Collaborative Innovation Center of Extreme Optics, Shanxi University, Taiyuan 030006*

(Received 4 February 2019)

Matter-wave interferometers with spin quantum states are attractive in quantum manipulation and precision measurements. Here, five spatial interference patterns corresponding to the full spin states are observed in each run of the experiment, by the combination of the Majorana transition according to the exponential modulation of the magnetic field pulse decline curve and radio frequency coupling among multiple magnetic sub-states. Compared to the realization of two Majorana transitions, the interference fringe for the magnetic field insensitive state also has a higher contrast. After spatially overlapping the full magnetic sub-state interference patterns dozens of times in consecutive experimental measurements, clear fringes are still observed, indicating the great stability of the relative phases of different components. This indicates the potential to achieve an interferometer with multiple spin clocks.

PACS: 03.75.Dg, 32.80.Qk, 02.30.Yy DOI: 10.1088/0256-307X/36/5/050301

Matter-wave interference has greatly promoted the development of fundamental quantum science, precision metrology, and atomic and molecular physics,[1–3] since the interference between two condensates was reported in 1997.[4] The 'spinor condensates', subject to magnetic and superfluid interactions, involve even more interesting effects, such as quantum phase coherence, long-range ordering, and symmetry destruction.[5–7] Furthermore, a multi-spin Bose–Einstein condensate (BEC) system, in which entanglement of internal and external degrees of freedom[8] as well as internal magnetic dipole interactions exist,[9] has exhibited exotic phenomena different from scalar quantum fluids.

Multi-spin interferometers based on the spinor states have recently attracted more attention due to, for example, the coherence of multiple-path interference,[10,11] the macroscopic spin polarization between independent spin states,[12] and the atomic clock interferometer to study the interplay of general relativity and quantum physics.[13,14] They can also be used to measure external fields whose interactions with atoms are state-sensitive, and the interferometer sensitivity improves with the number of paths.[15,16] This kind of interferometer requires coherent manipulation of internal states. The normal method includes the Majorana method,[17,18] the radio frequency (rf) coupling method,[19,20] the Raman laser method,[21] and so on. We implement a parallel multi-component interferometer by combining two Majorana transitions.[22] However, the interference fringes of full spin states cannot be observed for the insensitive magnetic sub-state.

In this Letter, we combine Majorana transition and rf coupling to control the magnetic sub-states and observe interference fringes of all spin states in our double-slit interferometer. The initial atomic cloud is populated into two magnetic sub-states by the finely controlled Majorana transition, then the two magnetic sub-states are populated into five states respectively by the rf-induced Rabi pulse. With a fine-tuned procedure, space interference fringes in which all spin-state fringes overlap can be observed. We also take one step further to average the interference fringes in dozens of consecutive experiments and find that the interference patterns stay clear. This indicates the phase stability of multiple spin fringes, which is beneficial to the realization of an interferometer with multiple spin clocks.[13]

This scheme of the dual-path interferometer based on full spin states is shown in Fig. 1. The initial state $|\Psi\rangle$ is prepared at T_0, which is then transferred to two magnetic sub-states $|\Psi_+\rangle$ and $|\Psi_-\rangle$ through a Majorana transition. After $|\Psi_\pm\rangle$ undergo different evolution paths, they are transferred to all magnetic sub-states $|\Psi_{\pm,m_F}\rangle$ by rf coupling, where the two copies of each state can interfere with each other.[23] The time-of-flight (TOF) pictures in the plane (y, z) of all states mentioned above are depicted above the time line in Fig. 1(a). The details of our scheme are described in the following.

Figure 1(b) shows the time diagrams of the multi-spin interferometer implementation. (1) Using the finely controlled non-adiabatic Majorana transition pulse with the duration t_1, as shown in Fig. 1(b2), the beam splitter implements the transition from $|\Psi\rangle$ state to $|\Psi_+\rangle + |\Psi_-\rangle$. (2) Under the state-dependent force of the gradient magnetic field B'_y, as shown in Fig. 1(b1), the path difference of $|\Psi_+\rangle$ and $|\Psi_-\rangle$ wave packets is accumulated with the Stern–Gerlach pro-

*Supported by the National Key Research and Development Program of China under Grant No 2016YFA0301501, and the National Natural Science Foundation of China under Grant Nos 61727819 and 91736208.

**Corresponding author. Email: xjzhou@pku.edu.cn

© 2019 Chinese Physical Society and IOP Publishing Ltd

cess of the duration t_2, and we have

$$\Psi_q(y) = \Psi(y)e^{iq\kappa y/2}|q\rangle, \quad (1)$$

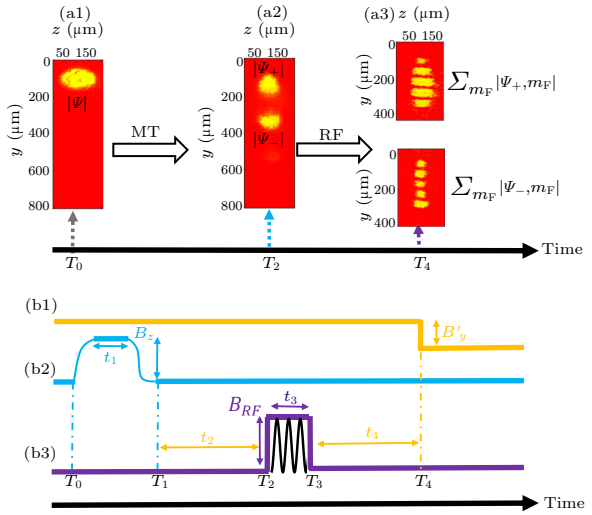

Fig. 1. (a) The scheme to the dual-path interferometer based on full spin states by the Majorana transition method and the rf coupling method. (b) Experimental time diagrams. (b1) The gradient magnetic field B'_y along the y direction, which is provided by the quadruple magnetic field. (b2) The Majorana pulse which includes the adiabatic rising and t_1 keeping time of the magnetic field and the finely tuned decline curve. Here B_z is the magnetic field strength, which is supplied by the Helmholtz coil along the z direction. (b3) The purple one represents the rf pulse, and $B_{\rm rf}$ is the rf pulse amplitude.

The qth copy ($q = \pm$) marks two copies of the atomic cloud before the rf pulse, $\Psi(y)$ is a (one-dimensional) localized normalized wave function, and κ is the relative wave vector of the two copies, which is mainly influenced by the t_2 process. (3) Adding the rf pulse with duration t_3 (as shown in Fig. 1(b3)) to the superposition states, each state is transferred into all magnetic sub-states. There are five states corresponding to the spin $F = 2$. (4) After the Stern–Gerlach process with duration t_4 and TOF, we have

$$\Psi_q(y) = \frac{1}{\sqrt{5}}\Psi(y)e^{iq\kappa y/2}\sum_{m_F=-2}^{2} e^{iq\phi_{m_F}/2}|m_F\rangle, \quad (2)$$

where ϕ_{m_F} is the phase difference of the two copies $|\Psi_{+,m_F}\rangle$ and $|\Psi_{-,m_F}\rangle$. By adjusting the time of the two Stern–Gerlach processes, the overlap of the same component wave packets and the separation of different component wave packets are achieved. The recombination of the same component wave packets by the external momentum transforms their relative phase difference into the interference pattern.

We prepare a BEC of ^{87}Rb in state $|F, m_F\rangle = |2, 2\rangle$ in a hybrid trap, where the spin $F = 2$, and the magnetic sub-state $m_F = 2$. The hybrid trap is formed by the overlap of a single-beam optical dipole trap with the wavelength 1064 nm and a quadruple magnetic trap. A nearly-pure condensate of about 1.0×10^5 atoms with the temperature 50 nK is achieved with the harmonic trapping frequencies $(w_x, w_y, w_z) = 2\pi \times (28\,\text{Hz}, 55\,\text{Hz}, 65\,\text{Hz})$, respectively. The BEC is localized 158 μm below the center of the quadruple magnetic trap, which provides a gradient magnetic field ($B'_y = 12.4\,\text{G/cm}$) at the bottom of the trap and hundreds of milligauss magnetic field strength at the position of the BEC. Thus the weak magnetic field causes the magnetic sub-states of the ^{87}Rb atom to no longer degenerate, resulting in a Zeeman split at about 310 kHz.

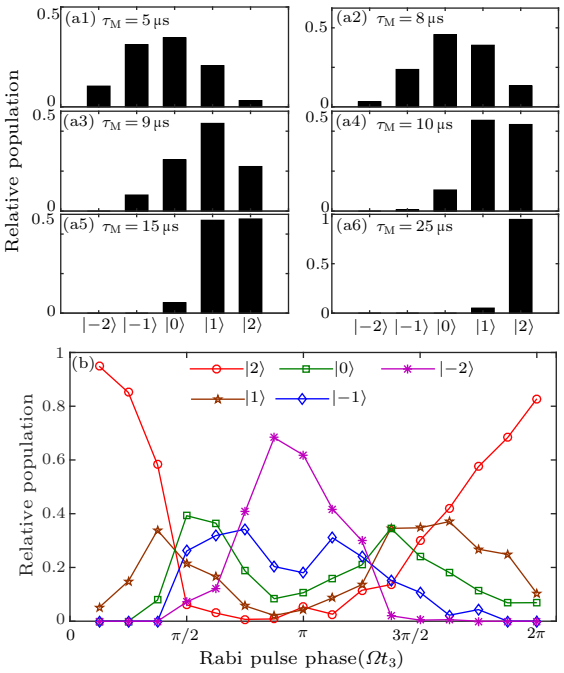

Fig. 2. The manipulation of the spin states, where the atom number for different spin states are obtained by absorption imaging after 1.3 ms Stern–Gerlach process and 26 ms TOF. (a) The atom population in the five spin states versus the falling time factor τ_M of the non-adiabatic Majorana transition. (b) Population transfer by the Rabi pulse which is achieved by opening the timing sequences in Figs. 1(b1) and 1(b3), where the five different states $|2\rangle$, $|1\rangle$, $|0\rangle$, $|-1\rangle$ and $|-2\rangle$ are given by the red, dark blue, light blue, green, and black points, respectively.

Although non-adiabatic transitions of atoms within magnetic sub-states have been a concern of the community for a long time,[17,18] precise control of Majorana transition is still difficult to realize. In our experiment, the pulse (as shown in Fig. 1(b2)) to control spin flips is achieved by the finely controlled decline curve. The adiabatic rising time of the pulse is 40 μs and the keeping time of B_z is $t_1 = 20\,\mu s$. To improve the control accuracy and stability of the magnetic field rotation and to reduce the magnetic field oscillation at the beginning and the end of the decline curve, we design the decline curve using

$$C_M = B_z e^{-3(t/\tau_M)^2}, \quad (3)$$

where B_z is the magnetic field strength (about 1 Gauss) in the position of the BEC along the z direction supplied by the additional Helmholtz coil with

the current of 1.1 A, and the time factor $\tau_{\rm M}$ decides the rotation speed of the magnetic field.

In the diagram of Figs. 1(b1) and 1(b2), by controlling different falling times $\tau_{\rm M}$, the $|2\rangle$ state atoms can be populated into different magnetic sub-states with different populations, as shown in Fig. 2(a). When $\tau_{\rm M} = 15\,\mu$s, it populates the initial state approximately equally into $|2\rangle(49\%)$ and $|1\rangle(48\%)$, leaving only a few atoms (3%) in $|0\rangle$, as depicted in Fig. 2(a5), which can be seen as a one-two beam splitter.

The rf pulse is generated by the signal generator Agilent 33521A connected to the rf coil. The phase of each pulse was locked to its trigger. The frequency was set to the resonant frequency 310 kHz to match the Zeeman split between the sub-levels in the magnetic trap, and the pulse amplitude $B_{\rm rf}$ is kept constant, which is decided by the rf power. Figure 2(b) shows the population transfer with the Rabi pulse phase Ωt_3 among five Zeeman states, where Ω is the Rabi frequency. The pulse duration t_3 is the integer multiple of two cycles for the resonant frequency in each run. The π Rabi pulse transfers the population between $m_F = 2$ and $m_F = -2$ states, while the $\pi/2$ pulse completes the symmetric population, which means the pulse can be seen as a one-fifth beam splitter. We note that the same results can be obtained by changing the Rabi pulse amplitude $B_{\rm rf}$ and keeping the duration-amplitude product constant.[16]

According to Fig. 2(b), when the $|2\rangle$ and $|1\rangle$ states have a similar atomic population, the $|0\rangle$ state has nearly 20% occupation. Comparing Figs. 2(a) and 2(b), we find that the Majorana transition process with $\tau_{\rm M} = 15\,\mu$s is the optimal choice to transfer the initial state to $|m_F = 2\rangle$ and $|m_F = 1\rangle$ equally with almost negligible $|m_F = 0\rangle$ occupation, which can effectively suppress the effects of the multipath.[10,24] That is why we use the Majorana transition as a one-two beam splitter in our first step.

Through the time sequences in Fig. 1(b), we can observe the separation of all wave packets by the optimized Stern–Gerlach process with $t_2 = 3000\,\mu$s and $t_4 = 200\,\mu$s after 26 ms TOF. When $\tau_{\rm M} = 15\,\mu$s for Majorana transition and $\pi/2$ pulse for rf coupling are chosen, each state of $|\Psi_+\rangle$ and $|\Psi_-\rangle$ is divided into five wave packets of $m_F = 2, 1, 0, -1, -2$ from top to bottom with similar proportion, as shown in Fig. 1(a3), which means that the rf coupling as a one-fifth beam splitter in our second step is better than the Majorana transition.[22] Therefore, we have exhibited the feasibility to realize a dual-path manipulation of all sub-magnetic states simultaneously with the combination of Majorana transition and rf coupling.

The experimental data for the multi-component spatial interference fringes are shown by the black dots in Fig. 3, and are achieved by the time sequences in Fig. 1(b). Here we choose the Majorana transition decline curve factor $\tau_{\rm M} = 15\,\mu$s and rf pulse $\Omega t_3 = \pi/2$ ($t_3 = 27\,\mu$s) to achieve a uniform population of atoms in five magnetic sub-states. In the experiment, after the $|2, 2\rangle$ state is prepared, we turn off the optical trap to allow the condensate wave packet to expand through 2.2 ms for easier overlapping of interference,[22] and $T_0 = 2.2$ ms. As for the two Stern–Gerlach processes, we use a smaller $t_2 = 137.5\,\mu$s and a larger $t_4 = 1300\,\mu$s, so that the same component wave packets can be overlapped and the different components are separated after TOF.

To show the visibility of the interference pattern clearly, we fit it by the following function[22]

$$\Lambda_{m_F} = A_{m_F} \cdot G_{m_F}(y)\Big[1 + V_{m_F} \cos\Big(\frac{2\pi}{\lambda_{m_F}} y + \phi_{m_F}\Big)\Big], \tag{4}$$

where A_{m_F} is the amplitude of the Gaussian wave packet $G_{m_F}(y)$, the cosine function represents the interference pattern, λ_{m_F} and ϕ_{m_F} are the fringe spacing and the initial phase of the fringe, and V_{m_F} denotes the visibility of the interference pattern.

From the fitting, we know that the visibility for states $|2\rangle$, $|-2\rangle$, and $|1\rangle$ is about 0.75, and for the state $|-1\rangle itis 0.45$. The visibility is 0.43 for the insensitive magnetic state $|0\rangle$, which is much higher than the contrast $V_0 = 0.14$ by the two Majorana transitions.[22] The fringe spacing for $|2\rangle$, $|1\rangle$, and $|-1\rangle$ is 27.2 μm, and for the magnetic repelled state $|-2\rangle$ it is 27.9 μm. However, this spacing becomes 28.9 μm for the state $|0\rangle$. From the results we know that by the combination of the Majorana transition and the rf method, we can obtain matter-wave interferometers of the full spin states at the same time.

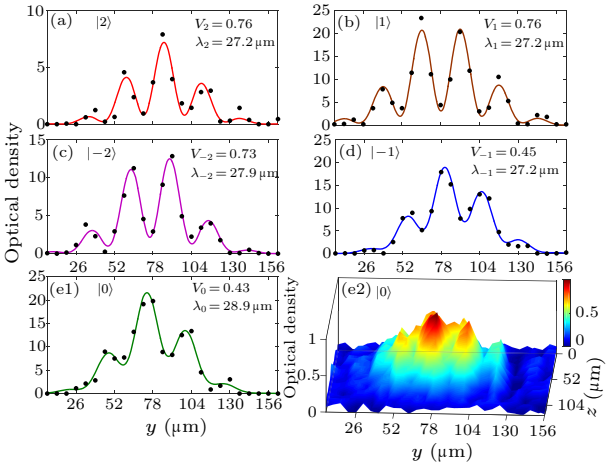

Fig. 3. The five spin interference fringes by the combination of Majorana transition and the rf coupling method, where the black dots are the experimental data along the z-direction integration of the different spin states in the same experiment and the solid lines are the fitting curves by equation (4). (a)–(e1) The interference fringes of $|2\rangle$, $|1\rangle$, $|-2\rangle$, $|-1\rangle$, and $|0\rangle$, respectively. (e2) The TOF image for $|0\rangle$ corresponding to (e1) by the absorption imaging method.

Dual-path interference based on multi-spin states is important for improving the sensitivity of interferometry,[25–28] while the stable phase relationship among multi-spin interference is the premise of realizing a clock interferometer.[13] We can investigate this by overlapping the multi-spin interference fringes

after reasonably selecting different times (t_2 and t_4) of the Stern–Gerlach process from those of the separated interference fringes in Fig. 3. The relative phase information between multi-spin interferences is reflected by the contrast of overlapping interference fringes.

The sum of states corresponding to the interference of two wave packets can be written as

$$|\Psi_+(y) + \Psi_-(y)|^2 = |\Psi(y)|^2 \sum_{m_F=-2}^{2} \left[1 + \cos\left(\frac{2\pi y}{\lambda_{m_F}} + \phi_{m_F}\right)\right]/5. \quad (5)$$

It represents a linear superposition of two-path interference of five magnetic sub-states, where $\lambda_{m_F} = 2\pi/\kappa$ is the fringe spacing of the interference fringes. Since T_4 is short, B'_y can be considered as a constant, and the wave vector κ for different spin states stays the same. The phase ϕ_{m_F} is mainly influenced by two Stern–Gerlach processes, Majorana transitions and rf coupling.

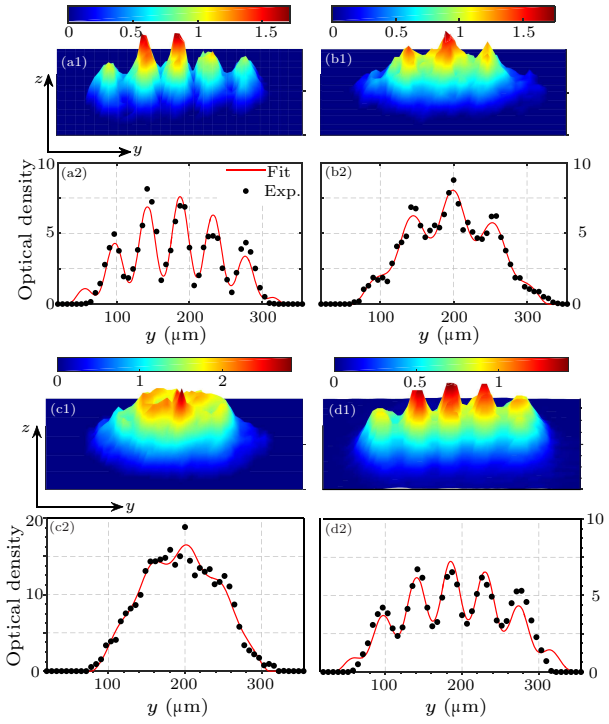

Fig. 4. The overlap of all magnetic sub-state fringes. (a1)–(c1) The overlap of five interference fringes tested in a single experiment after TOF by different Stern–Gerlach processes. (d1) The average of 23 consecutive experimental data samples under (a1) conditions to demonstrate the coherence of the state population operation. (a2)–(d2) Fit to (a1)–(d1) by equation (6), where the black points are the experimental data integrated along the z direction, and the red line is the fitting curve. The contrast decreases from 0.55 (a2) to 0.35 (d2) after the average.

Since the evolution time in the trap in the realization of overlap of multi-component interference fringes is much shorter than the separated fringes, the wave packet $\Psi(y)$ can be regarded as a Thomas–Fermi envelope,[29] then equation (5) reads

$$\Lambda_m = A_m \cdot T_F(y)\left[1 + V\cos\left(\frac{2\pi}{\lambda}y + \varphi\right)\right], \quad (6)$$

where A_m is the amplitude of the Thomas–Fermi wave packet $T_F(y) = \max\{1 - (y - y_0)^2/2\sigma^2, 0\}^{3/2}$ with y_0 being the center of the atom cloud and σ being the width of the wave packet, and φ is the overall phase.

When the differences of each pair of the five fringe phases ϕ_{m_F} are the integer multiple of 2π, there will be a contrast $V = 1$ in theory, which can be achieved by adjusting t_2 and t_4 appropriately. As shown in Fig. 4(a1), we can observe clear overlapping interference fringes when $t_2 = 8\,\mu s$ and $t_4 = 133\,\mu s$. Integrating the data in Fig. 4(a1) along the z direction and fitting it by equation (6), it is known that it still has a high contrast $V = 0.55$ with a fringe spacing of $\lambda = 46\,\mu m$. However, when the phase differences between ϕ_{m_F} are not all 2π integers, the contrast reduces to $V = 0.24$ (with $\lambda = 58\,\mu m$) as shown in Figs. 4(b1) and 4(b2), with $t_2 = 18\,\mu s$ and $t_4 = 146\,\mu s$. When all the fringes are complementary in space, the contrast reduces to $V = 0$ as shown in Figs. 4(c1) and 4(c2), in which $t_2 = 28\,\mu s$ and $t_4 = 146\,\mu s$.

The contrast for the average of the 23 consecutive experimental data samples in Fig. 4(a2) ($V = 0.55$) reduces to 0.35 as shown in Fig. 4(d2). This decrease is mainly due to the noise in the process of rf coupling, Majorana transition, and the interaction between the gradient magnetic field B'_y and different spin states, as well as the offset of the interference fringe packet position. Meanwhile, the interference fringes are still observed in an average of multiple experiment measurements, indicating the stability of the difference of phase ϕ_{m_F} of multiple spin fringes, which means that the experimental operation is coherent.

In summary, according to the optimal fine-manipulation Majorana transition by the exponential modulation of the magnetic field pulse decline curve, we successfully transfer atoms from one spin state to two states with approximately equal population while the population of the other spin state remains nearly zero. We then populate atoms from the two spin states to all five spin states with the help of the rf-induced Rabi pulse. Through the combination of these two methods, the spatial interference fringes of the full magnetic sub-states are realized, and the clear interference fringe for the magnetic field insensitive state is also observed. By controlling the Stern–Gerlach process, the spatial overlap fringes of five fringes corresponding to the spin $F = 2$ can be observed and the overlapping interference fringe still shows a high contrast after averaging over dozens of consecutive experimental TOF images. This indicates the coherence of this experimental operation, and provides the possibility to achieve an interferometer with five spin clocks.

We thank Heng Fan, Baoguo Yang, Ji Li, Peng Zhang, and Xinhao Zou for helpful discussions.

References

[1] Cronin A D, Schmiedmayer J and Pritchard D E 2009 *Rev. Mod. Phys.* **81** 1051
[2] Hu D, Niu L X, Jin S J, Chen X Z, Dong G J, Schmiedmayer J and Zhou X J 2018 *Commun. Phys.* **1** 29
[3] Niu L X, Jin S J, Chen X Z, Li X P and Zhou X J 2018 *Phys. Rev. Lett.* **121** 265301
[4] Andrews M R, Townsend C G, Miesner H, Durfee D S, Kurn D M and Ketterle W 1997 *Science* **275** 637
[5] Stamper-Kurn D M and Ueda M 2013 *Rev. Mod. Phys.* **85** 1191
[6] Hall D, Matthews M, Wieman C and Cornell E A 1998 *Phys. Rev. Lett.* **81** 1543
[7] Eto Y, Shibayama H, Saito H and Hirano T 2018 *Phys. Rev. A* **97** 021602
[8] Machluf S, Japha Y and Folman R 2013 *Nat. Commun.* **4** 2424
[9] Eto Y, Saito H and Hirano T 2014 *Phys. Rev. Lett.* **112** 185301
[10] Von Prillwitz K, Rudnicki L and Mintert F 2015 *Phys. Rev. A* **92** 052114
[11] Paul T and Qureshi T 2017 *Phys. Rev. A* **95** 042110
[12] Wheeler M H, Mertes K M, Erwin J D and Hall D S 2004 *Phys. Rev. Lett.* **93** 170402
[13] Margalit Y, Zhou Z F, Machluf S, Rohrlich D, Japha Y and Folman R 2015 *Science* **349** 1205
[14] Pikovski I, Zych M, Costa F and Brukner Č 2017 *New J. Phys.* **19** 025011
[15] Schmiedmayer J, Ekstrom C R, Chapman M S, Hammond T D and Pritchard D E 1994 *J. Phys. II* **4** 2029
[16] Petrovic J, Herrera I, Lombardi P, Schaefer F and Cataliotti F S 2013 *New J. Phys.* **15** 043002
[17] Ma X Q, Xia L, Yang F, Zhou X J, Wang Y Q, Guo H and Chen X Z 2006 *Phys. Rev. A* **73** 013624
[18] Xia L, Xu X, Guo R, Yang F, Xiong W, Li J T, Ma Q L, Zhou X J, Guo H and Chen X Z 2008 *Phys. Rev. A* **77** 043622
[19] Lovecchio C, Schäfer F, Cherukattil S, Alì Khan M, Herrera I, Cataliotti F S, Calarco T, Montangero S and Caruso F 2016 *Phys. Rev. A* **93** 010304
[20] Lovecchio C, Cherukattil S, Cilenti B, Herrera I, Cataliotti F S, Montangero S, Calarco T and Caruso F 2015 *New J. Phys.* **17** 093024
[21] Lombardi P, Schaefer F, Herrera I, Cherukattil S, Petrovic J, Lovecchio C, Marin F and Cataliotti F 2014 *Opt. Express* **22** 19141
[22] Tang P J, Peng P, Li Z H, Chen X Z, Li X P and Zhou X J 2018 arXiv:1810.05332[hep-ph] [cond-mat.quant-gas]
[23] Fort C, Maddaloni P, Minardi F, Modugno M and Inguscio M 2001 *Opt. Lett.* **26** 1039
[24] Lu S B, Yao Z W, Li R B, Luo J, Barthwal S, Chen H H, Lu Z X, Wang J and Zhan M S 2018 *Opt. Commun.* **429** 158
[25] Mitchell M W, Lundeen J S and Steinberg A M 2004 *Nature* **429** 161
[26] Weihs G, Reck M, Weinfurter H and Zeilinger A 1996 *Opt. Lett.* **21** 302
[27] Weitz M, Heupel T and Hänsch T 1996 *Phys. Rev. Lett.* **77** 2356
[28] Gross C, Zibold T, Nicklas E, Estève J and Oberthaler M K 2010 *Nature* **464** 1165
[29] Dalfovo F, Giorgini S, Pitaevskii L P and Stringari S 1999 *Rev. Mod. Phys.* **71** 463